Ceramics International 45 (2019) 5259–5265

Contents lists available at ScienceDirect

Ceramics International

journal homepage: www.elsevier.com/locate/ceramint

Size effect on magnetic properties of $Zn_{0.95-x}Mg_xNi_{0.05}O$ nanoparticles by Monte Carlo simulation

I.P. Duru[a], E. Ozugurlu[b], L. Arda[c,*]

[a] Marmara University, Department of Physics, 34722, Istanbul, Turkey
[b] Istanbul Technical University, Faculty of Science and Letters, Department of Mathematics, 34469, Istanbul, Turkey
[c] Bahcesehir University, Faculty of Engineering & Natural Sciences, Department of Mechatronics, 34349 Istanbul, Turkey

ARTICLE INFO

Keywords:
Diluted magnetic semiconductor
Exchange-bias
Monte Carlo simulation
Room temperature ferromagnetism

ABSTRACT

Diluted magnetic semiconductors (DMSs) have been providing a wide research area with various conflicting results of magnetic properties which are generally originated from structural characteristics due to fabrication process. We focused on the size dependent magnetic behavior of $Zn_{0.95-x}Mg_xNi_{0.05}O$ nanoparticles as a promising *novae material* introducing room temperature ferromagnetism (FM) at low doping concentrations of Mg^{+2} and Ni^{+2} ions. Markov Chain Monte Carlo method based on Metropolis algorithm is used to simulate the system, constructed on experimental parameters such as particle size (D), lattice constants (a and c), uniaxial anisotropy constant (K), applied field (H) herewith doping concentrations of Ni (5%) and Mg (1%). However, we described the system with the Heisenberg Hamiltonian to represent the exotic nature of the DMS type materials since determining the J_{ij} constants by tracing the type of the exchange relation between different types of atoms as reported in former studies. In the light of hysteresis measurements, nanoparticles generated between $5 < D < 15$ nm showed strong FM among others. An exciting result is that $D = 5$ nm, 10 nm and 15 nm curves are so close to be overlapped. Saturation magnetization (Ms) and coercive field (H_c) had peaks of; $D = 15$ nm remnant magnetization (Mr) increased with increasing D up to 50 nm. Furthermore, $D < 5$ nm and $D > 15$ nm sized particles started to lose FM behavior. In addition, magnetic features of $Zn_{0.95-x}Mg_xNi_{0.05}O$ nanoparticles can be controlled via picking a fabrication method to tune the particle size.

1. Introduction

Zinc oxide (ZnO) and ZnO-based nanoparticles, thin films, nanorod semiconductors have been playing an important role in many industrial applications such as spintronics, biomaterials, optical and magnetic memory devices, heat protecting windows, solar cells and sensors due to the wide-band gap with an energy gap of 3.37 eV, high electrochemical stability, absence of toxicity, good mechanical strength, and a large exciton binding energy of 60 meV at room temperature (RT) [1,2].

Recent studies show that doping ZnO with small amounts of magnetic Transition-Metals (TM) (Cr, Ni, Mn, Co, Fe and V) and rare earth elements (Yb, Er, Gd, Ho) form the Dilute Magnetic Semiconductors (DMSs) and are used in the spintronic applications. Wide-band gap semiconductors by achieving high Curie temperatures was focused [3]. After their prediction of the possibility of above RT ferromagnetism, the origin of magnetism in the DMS materials, correlation of magnetic properties with the transition metals, rare earth elements, and deep level doping and co-doping concentrations have been a great focus of the researchers. Moreover, DMS materials could be tuned like a band gap which affects the properties and applications of DMSs. When ZnO is doped with a suitable Mg which has a band gap of 7.8 eV, cubic crystal structure, and the ionic radius of Mg^{+2} (0.57 Å) is similar to that of Zn^{+2} (0.60 Å) [4]. We previously studied the structural properties of $Zn_{1-x}Mg_xO$ nanomaterials and showed that up to $x < 0.25$, Mg replaces Zn substitutionally yielding ZnMgO single phase and it is possible to obtain a ternary ZnMgO alloy with a wider band gap [5]. The Ni^{2+} (ionic radius = 0.69 Å) - doped ZnO might also be considered one of the most promising DMSs for RT ferromagnetism due to its ability to combine optical transparency and ferromagnetism among the transition metals. Highly Ni doped ZnO nano-crystalline ($Zn_{1-x}Ni_xO$, where x = 0, 0.1, 0.15, 0.2, 0.3) particles were synthesized using the sol–gel technique [6]. They found that samples exhibited the room-temperature ferromagnetism at 300 K. They also showed that the sizes of the nanoparticles decreased with increasing the doping concentrations and stated that the specific magnetization values might have been increased with decreasing average particle size. Mg doped ZnO nanoparticles in

---

[*] Corresponding author.
E-mail address: lutfi.arda@eng.bau.edu.tr (L. Arda).

https://doi.org/10.1016/j.ceramint.2018.11.223
Received 16 November 2018; Received in revised form 26 November 2018; Accepted 27 November 2018

Table 1
Concentration dependent average particle sizes, lattice parameters and volumes of the unit cell.

Sample name	*D*(nm)	*a* (nm)	*c* (nm)	*c/a*	Volume, *V* (nm ^{3})
$Zn_{0.94}Mg_{0.01}Ni_{0.05}O$	26.22	0.3230	0.5206	1.611	0.047035
$Zn_{0.93}Mg_{0.02}Ni_{0.05}O$	25.78	0.3240	0.5204	1.606	0.047309
$Zn_{0.92}Mg_{0.03}Ni_{0.05}O$	25.12	0.3255	0.5201	1.597	0.047720
$Zn_{0.91}Mg_{0.04}Ni_{0.05}O$	24.96	0.3244	0.5200	1.602	0.047389
$Zn_{0.90}Mg_{0.05}Ni_{0.05}O$	24.90	0.3253	0.5195	1.596	0.047607

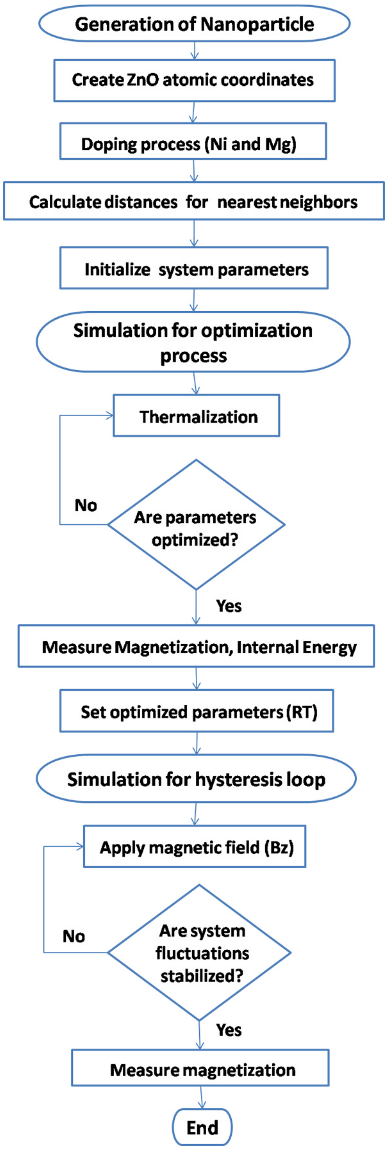

Fig. 1. Flow diagram of simulation process.

the range of 60–90 nm were produced [7] and they found that when the concentration of dopant was increased, morphology of structure changed. As Mg concentration value increases, the magnetization decreases significantly and the loop *M–H* curve at 300 K indicates the stronger ferromagnetism in $Zn_{0.94}Mg_{0.01}Ni_{0.05}O$ nanoparticles in the range of 24–27 nm within the percentages of 0.01 and 0.05 of Mg [8]. The size and shape of the nanoparticles depend on the preparation materials and methods. In the recent years, that is why researches have been focusing on highly ordered small nanoparticles of any scope, size and shape to advance in the area of modern nanotechnology [9].

In this study, apart from the usual approach to the magnetic interaction of two particles, we analyze the magnetic interaction between the dopant ion and the host based on the distance and type of the atom. The size effect on magnetic properties of Ni/Mg co-doped ZnO nanoparticles is investigated by Markov Chain-Monte Carlo (MC-MC) method and Metropolis algorithm [10]. We construct $Zn_{0.95-x}Mg_xNi_{0.05}O$ nanoparticles with experimental values of parameters such as lattice constants (a and c), uniaxial anisotropy constant (K) and applied field (H) [8].

2. The model and simulation

MC methods require remarkably large computational resources since a large number (millions to billions) of events called particles must be simulated to obtain a reasonably precise estimate of the quantities of interest (e.g., dose). To overcome these difficulties we used parallel computing techniques to obtain the data which was analyzed to calculate thermodynamic quantities and to display magnetic topographies of nanoparticles. The crystal structure of $Zn_{0.95\text{-}x}Mg_xNi_{0.05}O$ nanoparticles are constructed meticulously by considering whole atoms having the same spherical geometry. We use the experimental lattice constants, the average particle size and the volume of unit cell given [8] to optimize the system, see the Table 1.

In the beginning, ZnO atoms are arranged by considering the same crystal structure and labeled as Type 1 (Zn) and Type 2 (O). After that, following FM Ni atoms displaced via Zn atoms randomly through a constant doping concentration as 0.05 and labeled as Type 3 (Ni); paramagnetic (PM) Mg atoms are displaced with Zn. The Cartesian coordinates of hexagonal $Zn_{0.95-x}Mg_xNi_{0.05}O$ are obtained from the fractional coordinates which are constructed by a conversion operation Eq. (1) including the following lattice constants given in Table 1 [8]. In addition, the total number of atoms is determined with the change of the average particle size as Mg concentration increases. It enables us to mimic experimental process more realistically.

$$\begin{bmatrix} x \\ y \\ z \end{bmatrix} = \begin{bmatrix} a & b\cos\gamma & c\cos\beta \\ 0 & b\sin\gamma & c\dfrac{\cos\alpha-\cos\beta\cos\gamma}{\sin\gamma} \\ 0 & 0 & \dfrac{v}{ab\sin\gamma} \end{bmatrix} \begin{bmatrix} x_{frac} \\ y_{frac} \\ z_{frac} \end{bmatrix} \tag{1}$$

In Eq. (1), a, b, c, α, β, and γ are unit-cell parameters. v is the volume of unit-cell and is explicitly described by Eq. (2).

$$v = abc\sqrt{\sin^2\alpha - \cos^2\beta - \cos^2\gamma + 2\quad \cos\alpha\cos\beta\cos\gamma} \tag{2}$$

Crystal structure of hexagonal ZnO and $Zn_{0.95-x}Mg_xNi_{0.05}O$ are shown in Fig. 2b. and c, respectively. The Hamiltonian of the system is described by Eq. (3) where J_{ij} is the exchange coupling constant (different for all types) and H is external magnetic field along the z-direction. K is the uniaxial anisotropy constant and $\boldsymbol{u_i}$ is the unit vector of the magnetic anisotropy.

$$E = -\quad \sum J_{ij}(r_{ij})\boldsymbol{S}_i\boldsymbol{S}_j + D\sum\left[\frac{\boldsymbol{S}_i\boldsymbol{S}_k}{r_{ik}^3} - 3\frac{(\boldsymbol{S}_i\boldsymbol{r}_{ij})(\boldsymbol{S}_j\boldsymbol{r}_{jk}\Big)}{r_{ik}^5}\right] - K\sum(\boldsymbol{S}_i\boldsymbol{u}_i)^2 - H\sum S_i^z \tag{3}$$

Since the destructive effect was shown in [11], dipolar energy (second term in Hamiltonian) can be disregarded (D = 0) The first term in Eq. (3), exchange energy, determines the type of magnetic interaction (FM, AMF, etc.) between neighboring atoms. The first and second nearest neighbors are taken into account for both terms of Hamiltonian recognizing J which is lowered by the distance between atoms as $J_s = J_{ij} / r_{ij}$. The constants are set as having different values for all type of pair atoms such as Mg-Zn, Mg-Ni, etc. from the set of {Mg, Zn, Ni and O}.

In Fig. 1, flow diagram of the simulation process and Markov Chain Monte Carlo (MCMC) method is detailed [11]. We strictly split the

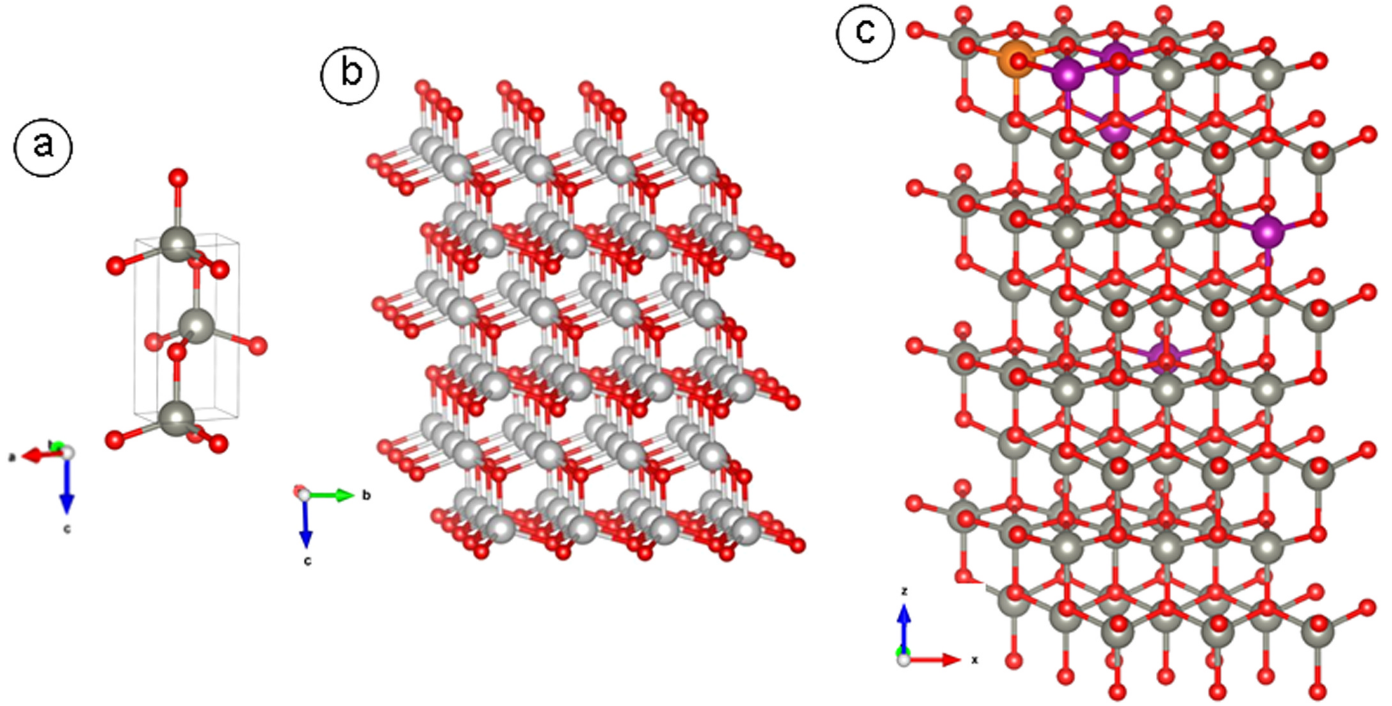

Fig. 2. (a) Unit-cell of ZnO (b) Super cell of ZnO (c) Crystal structure of $Zn_{0.95-x}Mg_xNi_{0.05}O$.

Table 2
Magnetic properties of Ni/Mg co-doped ZnO.

D (nm)	Ms (emu/atom)	Mr (emu/atom)	Hc ($\times10^4$Oe)
1	0.974671	0.047401	0.0019
2	0.976086	0.080589	0.0035
3	0.972239	0.122280	0.0049
4	0.978538	0.149757	0.0126
5	0.978964	0.215531	0.0121
10	0.978810	0.216609	0.0125
15	0.981153	0.224374	0.0329
25	0.983871	0.166217	0.01210
30	0.984827	0.140448	0.006745
50	0.98894	0.07590	0.006774

whole simulation process into 3 parts: generation of nanoparticle (mentioned in the beginning of this section), simulation of optimization process and simulation of hysteresis loops. Expectation values of thermodynamic quantities, observables as internal energy, specific heat and magnetic susceptibility are calculated after a considerable number of MCS (60% of total MCS) is used to reduce fluctuations. Unnecessary MCS moves may cause high spin-spin correlations. Therefore, total MCS number as 3×10^7 and the percentages (equilibrating system and calculating expectation value) are determined after several trials.

Finally, we formed hysteresis loops through the calculations of magnetization over whole atoms of the nanoparticle and setting particle sizes (D) and doping concentrations (x) mentioned in Table 1 under external uniform magnetic field along z-direction. Optimization process, especially determining suitable exchange constants between atoms of nanoparticle, leads us to enlighten the path for to figure out the size dependent magnetic properties of ZnMgNiO nanoparticles.

Metropolis algorithm is used to mimic the simulation process under the detailed balance condition. Calculating average magnetization at RT allowed us to form hysteresis loops for different size of nanoparticles such as D = 1, 2, 3, 4, 5, 10, 15, 25, 30 and 50 nm (different average particle sizes (D) and doping concentrations (x) between 0.01 and 0.05. Codes were written with C+ + programming language by testing each module in three different CPU architectures.

3. Results and discussion

At RT, FM property depends on the materials having parameters such as a preparation method and materials having a single phase. The preparation method of a material (nanoparticles, thin films, nanorod, etc.) determines the annealing process temperature and the size of the particle. In this study, we emphasize the known fact that when the size of the particle is determined, at the same time what preparation method should be used will be known as well. In Fig. 2, the unit and super cells of ZnO and the crystal structure of $Zn_{0.95-x}Mg_xNi_{0.05}O$ are given. VESTA visualization package [12] is preferred to illustrate the unit cell of hexagonal ZnO (Fig. 2a), supercell of ZnO including 100 Zn atoms (Fig. 2b), and randomly %5 Ni and %1 Mg doped to ZnO supercell (Fig. 2c) by experimentally obtained parameters which are also indicated in Table 1.

The magnetic properties of Ni/Mg co-doped ZnO nanoparticles are investigated by Markov Chain-Monte Carlo (MCMC) method and Metropolis algorithm [10] and the results are displayed in Table 2 and Figs. 3, 4, 6 and 7. Magnetization (M) versus applied magnetic field (H) plots are shown in Figs. 3 and 4 for particle sizes D = 1, 2, 3, 4, 5, 10, 15, 25, 30 and 50 nm (different average particle sizes). As seen in the Fig. 3, Fig. 4 and Table 2, nanoparticles showed FM properties for D values between 5 nm and 15 nm exhibiting maximum remnant magnetization (0.2243 emu/atom) and coercive field (0.329 kOe) thoroughly. However, for $D <$ 5 nm and $D >$ 15 nm, Mr, Ms, and Hc values decreased. Thus, FM property is also slightly decreased as shown in Table 2 and Fig. 5a–b. Fig. 6 and Fig. 8 show the plots of M-T under a field cooled (FC) and a zero-field (ZFC) condition in which the insets show the temperature dependent inverse susceptibility ($1/\chi$) curves for D= 1 nm, 5 nm and 50 nm. For the particle sizes D = 1 and 50 nm (i.e. $D <$ 5 nm), the systems behave like super paramagnetic (SPM) as expected [5], however for $D >$ 5 nm it is clearly FM. 1 kOe and 2 kOe external fields have been applied to obtain ZFC-FC and ($1/\chi$) curves respectively. We performed hysteresis measurements (Fig. 3 and Fig. 4) at RT (300 K) with applied field values between − 7 kOe and 7 kOe since it is sufficient to saturate the system.

According to the inset of Fig. 6, the Curie temperature for 5 nm nanoparticle is close to 600 K. The Curie temperatures estimated from

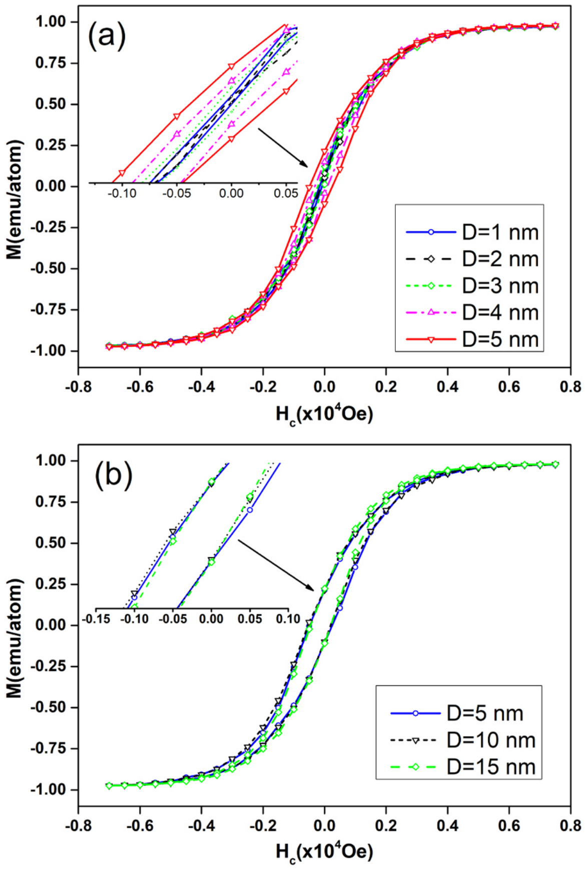

Fig. 3. M–H curves for (a) $D = 1$ nm (blue sphere solid line), 2 nm (black diamond dashed line), 3 nm (green diamond short dashed line), 4 nm (magenta up triangle dash dotted line) and 5 nm (red down triangle solid line) (b) $D = 5$ nm (blue sphere solid line), 10 nm (black down triangle short dashed line) and 15 nm (green diamond dashed line). (For interpretation of the references to color in this figure legend, the reader is referred to the web version of this article.)

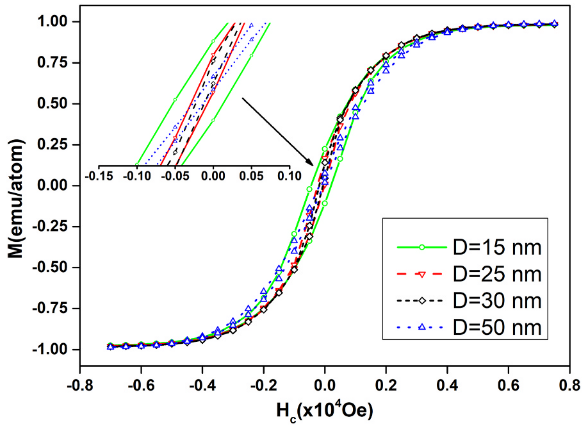

Fig. 4. M–H curves for D = 15 nm (green sphere solid line), 25 nm (red down triangle dashed line), 30 nm (black diamond short dashed line) and 50 nm (blue up triangle dotted line). (For interpretation of the references to color in this figure legend, the reader is referred to the web version of this article.)

intersection between T-axis and the asymptote of ($1/\chi$) curve for both ZFC-FC measurements and inset will be different from each other since $1/\chi$ values are calculated under 2 kOe external field. There is a slight splitting between FC and ZFC contributions as seen in Fig. 6.

As can be seen from Fig. 3 and 4, there is a clear hysteresis effect for most of the sample. The hysteresis loop significantly broadens for the particle sizes of 5 nm, 10 nm and 15 nm as well. However, although the width of the loops (coercive field) decreases for larger and smaller particles it does not completely diminishes. This means that the FM interactions still persist for almost all the particle sizes. Because the observed overall magnetization too large for any PM material and also saturates even relatively weak field that is not enough to saturate any PM sample. The field dependence of these curves is another indication for FM order as well. The M-S curve has a sharp S-shaped character that implies a strong molecular field (exchange interaction) making the sample FM at RT.

The particle size dependence of the calculated coercive field (that is responsible for the width of hysteresis loop), remnant magnetization and the saturation magnetization are given in Fig. 5. As can be seen from this figure, the change in saturation magnetization with the size of the particles is less than 1%. This means that the contributions to the magnetization do not change with the size of the particles. But the coercive field decreases for the size below 5 nm and above 25 nm and it exhibits a peak for the particle with the size of 15 nm. The remnant magnetization *Mr* behaves in consistent with the coercive field as well.

Actually the existence of coercive field is a clear indication to the FM, but converse is not necessarily true. It should be remembered that the hysteresis loop of soft FM materials is very narrow and coercive field is almost zero even for a strongly FM materials like supermalloy. The behavior of the hysteresis curves are influenced by many effects like crystalline anisotropy, impurities, crystal imperfections, kind of magnetizing processes (domain rotation of domain wall motion) etc. For instance, in the case of the geometric size of the magnetic particle is comparable to the magnetic domain size, as the applied field increased the parallel component of the macroscopic (measured- overall) magnetization gradually increases as a result of decreasing the angle between the domain magnetization and applied field vectors and finally saturates when all of the magnetic domains become completely parallel to the external field. But magnetostatic (Zeeman) energy of a single atomic moment in a PM sample is too small to overcome the thermal agitation energy to completely align itself parallel to an accessible field in any laboratory. Therefore, we can claim that all of our nanoparticles with different sizes exhibit FM (at least SPM) behavior and the interactions among the spins in a single particle are dominantly FM at RT.

The temperature dependence of macroscopic magnetization and analysis of the susceptibility concepts are critical to understand the magnetism of DMS. The temperature dependent M and inverse susceptibility ($1/\chi$) curves are shown in Figs. 6–9. As can bee seen from these figures, for FC case, the macroscopic magnetization for all particle sizes increases non-linearly with decreasing temperature, but these curves for ZFC cases pass a maximum at a certain temperature, T_c (canting) for each particle, and then start to sharply decrease again at lower temperatures. This temperature dependence is a characteristic property of so-called mictomagnetic (or spin-glass) like systems [13]. In all of this kind of systems, there are some AFM contributions in addition to the FM interactions between nearest and/or next nearest neighboring spins.

Besides, super exchange interaction may enlighten the origin of magnetic behavior (FM) of this type mixed states (FM-AFM) via pointing out the orbital (p-d) angles between unique parts (NiO, MgO, ZnO, ZnMg, ZnNi, etc) of the system [14]. As Goodenough-Kanamori-Andorson (GKA) had reported that two magnetic ions lying with 180° angle which had partially filled d shells show AFM behavior while 90° angled ions contribute to FM weakly [15]. Spin of unpaired electron of p orbital collaborate with ion's d orbital to determine the sign of the neighboring ions exchange interaction. It also depends on the occupancy of electrons to d orbital. In addition, s-d hybridization assist the magnetic behavior of the whole system after a threshold value for atomic clusters reached as reported [16]. However, magnetic moments of particles can decrease with decreasing sizes so the effect of Zeeman energy will naturally be reduced relative to the other interactions. It may also contribute to the overall magnetization for certain sizes such

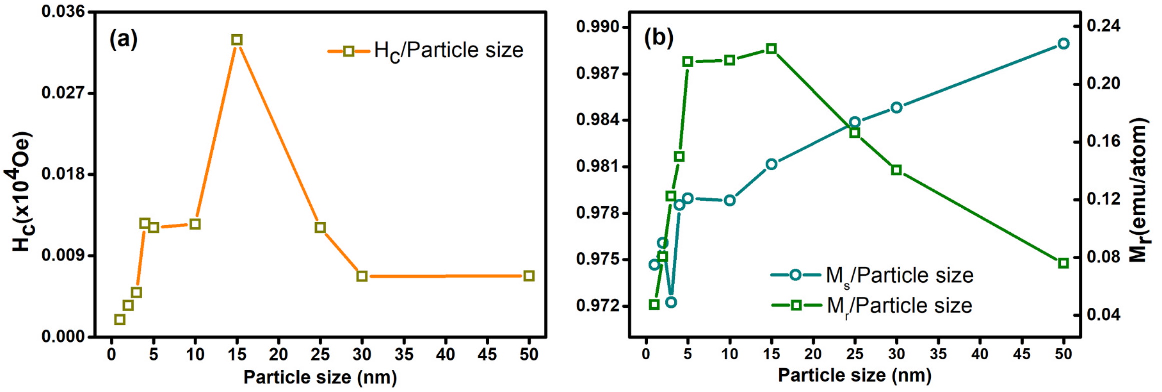

Fig. 5. (a) *Hc* coercive field/Particle size *D* (b) *Mr/Particle size* and *Ms*/Particle size *D* curves; dark cyan sphere solid line symbolize saturation magnetization where olive green square solid line represents the remnant magnetization. (For interpretation of the references to color in this figure legend, the reader is referred to the web version of this article.)

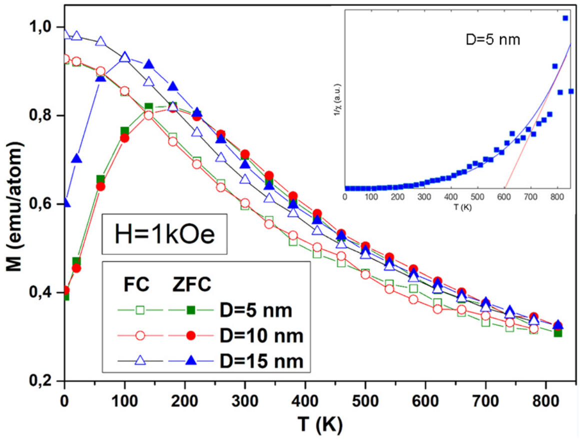

Fig. 6. Field cooling (FC) and zero field cooling (ZFC) *M* versus *T* curves for $D = 5$ nm, 10 nm and 15 nm. The inset gives the temperature dependent inverse susceptibility ($1/\chi$) curve for $D = 5$ nm.

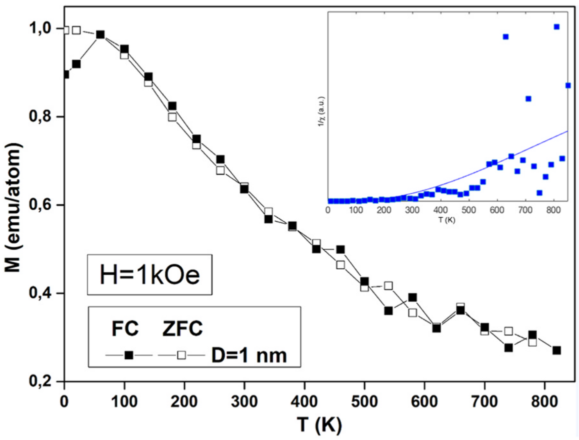

Fig. 7. Field cooling (FC) and zero field cooling (ZFC) curves for $D = 1$ nm. The inset gives the temperature dependent inverse susceptibility ($1/\chi$) curve.

as 5 nm, 10 nm and 15 nm. Competition between the FM-AFM interactions and anisotropic crystalline energy terms result in a spin canting especially below the Neel temperature for corresponding AFM interactions. Thus, the magnetization start to drop abruptly at the temperature below canting temperature T_c [17].

Regarding to the change of the T_c with the particle size; the particle size dependence of this temperature is quite similar to that of coercive field. As well known, the crystalline anisotropy is much stronger for the individual spins at the surface region of the particle compared to that for those in the bulk of the nanoparticles [18]. Therefore, as the particle size is decreased, the contribution to the total anisotropy can dominate to control the behavior of the total moment of the particle. For larger particles, magnetostatic energy (Zeeman) is large enough to control the overall magnetization. On the other hand, the thermal agitation is large enough to control spin freezing. Thus, spin canting (blocking temperature) becomes particle size-dependent.

In Fig. 9, we enlarged and plotted the temperature dependent inverse susceptibility ($1/\chi$) curves for $D = 5$ nm, 10 nm and 15 nm which are known as Curie-Weiss plots. We followed a non-linear curve fitting method called as the least-squares method. The inverse of susceptibility is fitted with the Eq. (4) in the least-squares sense.

$$1/\chi = AT^{\alpha}e^{BT} \tag{4}$$

The idea was to find the optimum *A* and *B* values by minimizing the sum of the squares of the residuals as given in Eq. (5). We used MATLAB's preexisting function ***fminsearch*** to find the optimum *A* and *B* values. We selected α values according to the data type. For example, for $D = 1$ nm, since $1/\chi$ values were close to zero, we took $\alpha = 3$ or $\alpha = 4$ to get a better fit (see Fig. 9 and Table 3). In Fig. 9, the solid line shows the least-squares fit for the raw data denoted by (*). The tangent line crosses the *T*-axis in the positive value indicating a FM material. However, for the particle sizes $D < 5$ nm or $D > 15$ nm we have observed that the inverse of susceptibility curves become linear if the Curie-Weiss law is obeyed indicating the PM material. The error in the least-squares sense was calculated according to the following formula:

$$E(A,\quad B) = \sum_{i=1}^{n}\left[AT_i^{\alpha}e^{BT_i} - \left(\frac{1}{\chi}\right)_i\right]^2 \tag{5}$$

We can see from Table 3 that we get large residual errors for $D = 1$ nm and $D = 50$ nm. The error amounts among $D = 5$ nm, 10 nm and 15 nm seemed very close to each other in the order of 10^{-5}.

In Fig. 9, for the particle sizes $D = 5$ nm, 10 nm and 15 nm, the Curie-Weiss temperature values are observed as 600 K, 590 K and 595 K, respectively, showing the FM behavior. In Fig. 8, for $D = 50$ nm, although the Curie-Weiss temperature is near to zero, least-squares approximation shows a positive value, however, note that the approximation had a large deviation as seen in Table 3, in the value of 1.7652 compared to 10^{-5}. FM behavior in ZnNiMgO nanoparticles can be explained in terms of the exchange interaction between the localized d spins on the transition metal ions and electrons from valence-band [19]. One can criticize the messy distribution of high temperature (HT) $1/\chi$ (scattered) values as large errors for $D = 50$ nm and $D = 1$ nm and moderate error for $D = 5$ nm, $D = 10$ nm and $D = 15$ nm sizes. We may

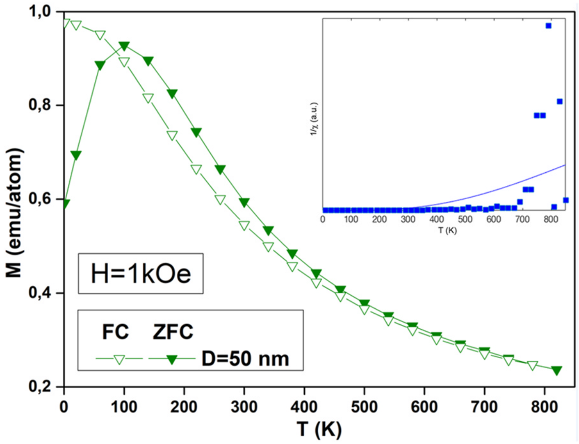

Fig. 8. Field cooling (FC) and zero field cooling (ZFC) curves for $D = 50$ nm. The inset gives the temperature dependent inverse susceptibility ($1/\chi$) curve.

predict such an error with increasing temperature and it is almost originated from suddenly increased classical correlations which are supposed to be mediated by high temperatures for magnetically stabilized sizes as $D = 5$ nm, 10 nm and 15 nm, whereas the probable source of this error cannot be procured by former arguments for $D = 50$ nm and $D = 1$ nm particle, too. Magnetization of small particles may be locked along one direction forming a single domain in contrast to $D >$ 15 sized particles. Latter ones contain several magnetic domains, as multi domain nanoparticles, especially a core-shell structure when saturated. However, note that messy points of $1/\chi$ at HT and fitting error are not interdependent.

Table 3
The curve fitting form of the functions $AT^{\alpha}e^{BT}$.

D (nm)	α	A	B	Error
1	3	0.5417	− 1.764	0.0447
5	2	0.0017	2.4179	7.7961×10^{-5}
10	2	0.0028	1.4158	2.9786×10^{-5}
15	2	0.0017	1.7663	8.989×10^{-6}
50	4	3.7169	− 2.2551	1.7652

Fig. 10 illustrates the z-projection of magnetic moments of $D = 15$ nm sized nanoparticle under certain applied fields $H = 0$, $H = 1$ kOe and $H = 7.5$ kOe which point *Mr*, low field magnetization and *Ms,* respectively. Blue regions represent the magnetic moments opposite to magnetization axis so red ones are parallel to $+z$ direction. Presence of magnetic domains (ZnO based nano materials) is greatly discussed [11]. They argue that the thermal agitations lead the domains to be anti-parallel to external field (blue regions) getting wider. In contrast to thermal effects formation of domains observed at certain temperature related to only strength of applied field. According to the Fig. 10a-b, domains changed the direction slightly by increasing external field. Fig. 10c visualizes the dominancy of applied high field resulting with the saturation of the system.

4. Conclusions

As a promising DMS structure, $Zn_{0.94}Mg_{0.01}Ni_{0.05}O$ nanoparticles are modeled, by constructing super-cell with experimental data [8], to investigate the size dependent magnetic behavior of these particles, theoretically. MCMC simulations are performed, firstly, for fitting

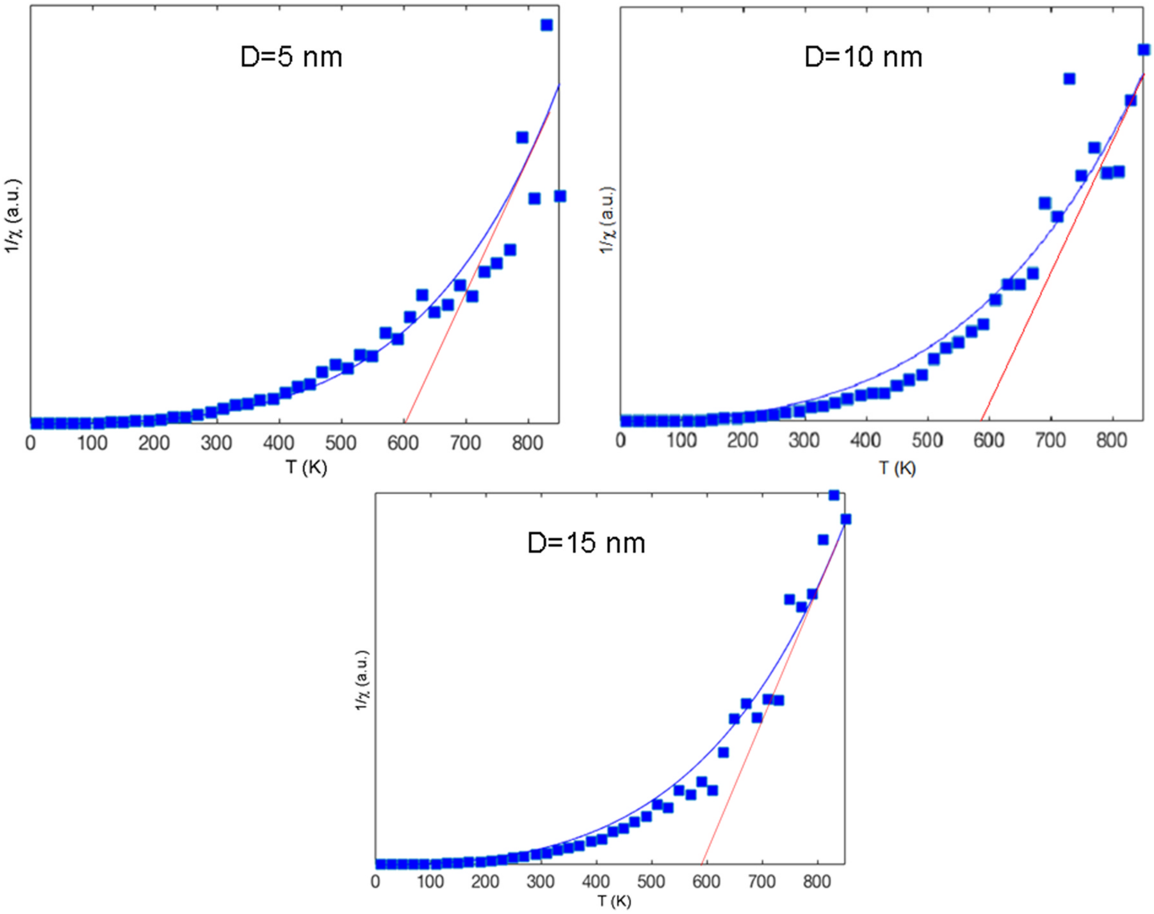

Fig. 9. The temperature dependent inverse susceptibility ($1/\chi$) curves for $D = 5$ nm, 10 nm and 15 nm.

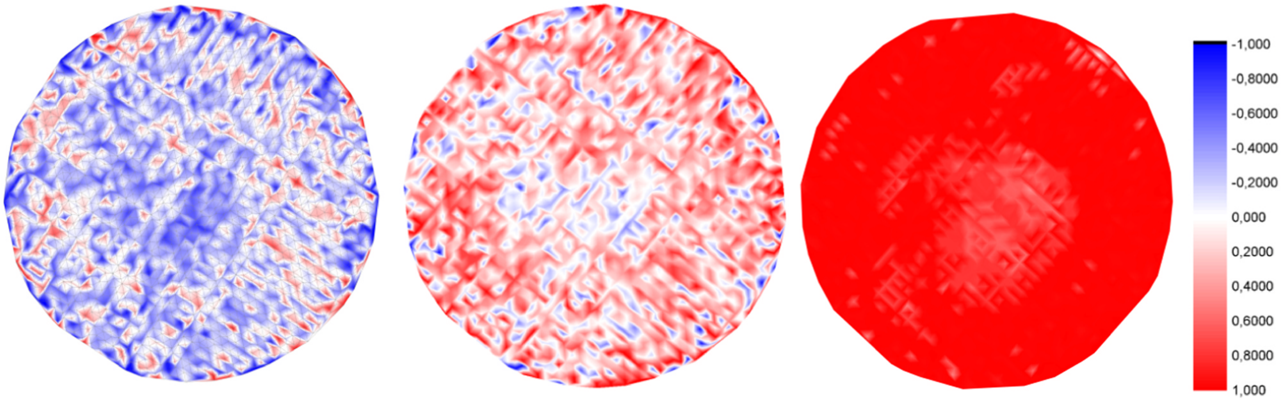

Fig. 10. Z-axis projection of magnetic moments of $Zn_{0.94}Mg_{0.01}Ni_{0.05}O$ with $D = 15$ nm under external fields (a) $H = 0$ (b) $H = 1$ kOe and (c) $H = 7.5$ kOe.

process with Heisenberg model [11] until DMS like behavior is observed ($D \approx 26$) and then for characterization of nanoparticles to figure out size dependent attitude of spherical shaped ZnMgNiO nanoparticles. We also simulated the system for $Zn_{0.94}Mg_{0.01}Ni_{0.05}O$ for different particle sizes both bigger and smaller than $D \approx 26$.

Our findings show that our simulations are parallel with the findings of the experimental data [8]. We conclude that for the particle sizes $D < 5$ nm, the systems behave like SPM, however, for $5 \leq D \leq 15$ it does clearly shows FM attitude. However, Curie-Weiss temperature values are found to be diversely where they decrease inversely proportional to increasing D. Moreover, larger nanoparticles as $D > 15$ nm, cause a gradual diminishment of FM behavior. It is obvious that magnetic domains change direction by increasing external field whereas the outer shell is fairly saturated. Furthermore, magnetization of inlying sub particles, diverge to zero forming a spinless core which is already mediated by saturation. Consequently, we found that the best FM was observed for D between 5 and 15 nm which should be considered for an option in production.

Acknowledgements

The authors would like to thank the Research Funds of Bahcesehir University (BAU-BAP.2018.02.16) for the supports.

References

[1] M. Gancheva, M. Markova-Velichkova, G. Atanasova, D. Kovacheva, I. Uzunov, R. Cukeva, Design and photocatalytic activity of nanosized zinc oxides, Appl. Surf. Sci. 368 (2016) 258–266, https://doi.org/10.1016/j.mssp.2017.10.025.

[2] Kai-Lin MunusamyThirumavalavan, Huang, Jiunn-Fwu Lee, Preparation and morphology studies of nano zinc oxide obtained using native and modified chitosans, Mater., MDPI 6 (9) (2013) 4198–4212, https://doi.org/10.3390/ma6094198.

[3] T. Dietl, H. Ohno, F. Matsukura, J. Cibert, D. Ferrand, Zener model description of ferromagnetism in zinc-blende magnetic semiconductors, Science 287 (2000) 1019–1022, https://doi.org/10.1126/science.287.5455.1019.

[4] J. Vidic, S. Stankic, F. Haque, D. Ciric, R. Le Goffic, A. Vidy, J. Jupille, B. Delmas, Selective antibacterial effects of mixed ZnMgO nanoparticles, J. Nanopart. Res 15 (5) (2013) 1595, https://doi.org/10.1007/s11051-013-1595-4.

[5] Vahak Marghussian, Magnetic properties of nano-glass ceramics, Nano-Glass Ceram. Process., Prop. Appl. (2015) 181–223, https://doi.org/10.1016/B978-0-323-35386-1.00004-9.

[6] N. Dogan, A. Bingolbali, L. Arda, Preparation, structure and magnetic characterization of Ni doped ZnO nano-particles, J. Magn. Mater. 373 (2015) 226–230, https://doi.org/10.1016/j.jmmm.2014.03.053.

[7] R. Viswanatha, Y. ArthobaNayaka, C.C. Vidyasagar, T.G. Venkatesh, Structural and optical properties of Mg doped ZnO nanoparticles, J. Chem. Pharm. Res. 4 (4) (2012) 1983–1989 (issn: 0975-7384 CODEN)(USA)(: JCPRC5).

[8] C. Boyraz, N. Doğan, L. Arda, Microstructure and magnetic behavior of (Mg/Ni) co-doped ZnO nanoparticles, Ceram. Int. 43 (17) (2017) 15986–15991, https://doi.org/10.1016/j.ceramint.2017.08.184.

[9] Agnieszka Kołodziejczak-Radzimska, Teofil Jesionowski, Zinc oxide— from synthesis to application: a review, Mater. MDPI 7 (4) (2014) 2833–2881, https://doi.org/10.3390/ma7042833.

[10] H.V. Anh, N.H. Cuong, N. Tu, L.M. Tuan, D.X. Nui, N.D. Dung, N.D.T. Kien, P.T. Huy, D.X. Viet, Understanding ferromagnetism in C-doped CdS: Monte Carlo simulation, J. Alloy. Compd. 695 (2017) 1624–1630, https://doi.org/10.1016/j.jallcom.2016.10.308.

[11] I.P. Duru, C. Değer, T. Kalayci, M. Arucu, A computational study on magnetic effects of Zn1 − xCrxO type diluted magnetic semiconductor, J. Magn. Magn. Mater. 396 (2015) 268–274, https://doi.org/10.1016/j.jmmm.2015.08.031.

[12] K. Momma, F. Izumi, VESTA 3 for three-dimensional visualization of crystal, volumetric and morphology data, J. Appl. Crystallogr. 44 (2011) 1272–1276, https://doi.org/10.1107/S0021889811038970.

[13] B. Aktaş, Clear evidence for field induced unidirectional exchange surface anisotropy in NiMn alloys, Solid State Commun. 87 (11) (1993) 1067–1071, https://doi.org/10.1016/0038-1098(93)90562-2.

[14] J. Nogués, I.K. Schuller, Exchange bias, J. Magn. Magn. Mater. 192 (2) (1999) 203–232, https://doi.org/10.1016/S0304-8853(98)00266-2.

[15] J.B. Goodenough, Magnetism and the Chemical Bond, Interscience Publishers, New York-London, 1963.

[16] Shu-Rong Liu, Hua-Jin Zhai, Lai-Sheng Wang, s-d hybridization and evolution of the electronic and magnetic properties in small Co and Ni clusters, Phys. Rev. B 65 (2002) 113401, https://doi.org/10.1103/PhysRevB.65.113401.

[17] Y. Öner, B. Aktaş, Magnetization measurements and computer simulations for the magnetic hysteresis losses of reentrant $Ni_{100\text{-}x}Mn_xPt$ and Ni-Mn alloys, Phys. Rev. B 42 (4) (1990) 2425, https://doi.org/10.1103/PhysRevB.42.2425.

[18] Soshin Chikazumi, Physics of Ferromagnetism, 2nd ed., Clarendon Press, Oxford, 1977.

[19] T. Dietl, Ferromagnetic semiconductors, Semicond. Sci. Technol. 17 (4) (2002) 377–392, https://doi.org/10.1088/0268-1242/17/4/310.